CTF VOID DRIFT VALIDATION

M. Gergar and M. Avramova
The Pennsylvania State University
137 Reber Building, State College, PA 16801, USA
msg5123@psu.edu; mna109@psu.edu

R. Salko
Oak Ridge National Laboratory
Oak Ridge, TN 37831, USA
salkork@ornl.gov

ABSTRACT

CTF, a version of the thermal-hydraulic subchannel code COBRA-TF being jointly developed by The Pennsylvania State University (PSU) and Oak Ridge National Laboratory (ORNL) for applications in the Consortium for Advanced Simulation of Light Water Reactors (CASL), has been used to perform isothermal subchannel calculations in order to determine the void distribution in an experimental 2x2 rod bundle facility. The experiments were run with an air and water mixture as the working fluid in order to study the void drift phenomenon, which involves vapor bubbles migrating from small cross-sectional area subchannels to larger cross-sectional area subchannels. These simulations were performed in order to validate the void drift model used in CTF.

Since CTF does not directly solve the noncondensable gas conservation equations to obtain gas void (i.e., air in the air-water mixture), the inlet enthalpy of the CTF model was modified to from experimental values to sustain the desired vapor void fraction at the bundle inlet. The bundle average void fraction was then held constant with respect to axial location to simulate the noncondensa ble nature of air in the experiment by iterating the inlet fluid enthalpy. The modeling of the droplet flow field was disabled and the void distribution of the bundle was determined both with and without the void drift model enabled in order to demonstrate the efficacy of the model.

The CTF results calculated with the void drift option enabled exhibited the same trend as found in the experiment. Additionally, the average absolute error between the experimental and CTF results demonstrated that the corner subchannel void was consistently overpredicted while the center subchannel void was consistently underpredicted. However, the CTF-to-experiment error was consistently within the ±6% experimental error uncertainty when the void drift option was enabled. Conversely, the relative error was outside of this experimental uncertainty when the void drift modeling option was disabled.

KEYWORDS
CTF, Void Drift, Void Fraction

1. INTRODUCTION

Isothermal subchannel calculations using CTF were performed in order to determine the void distribution in a 2x2 rod bundle experimental facility. The motivation of these calculations was to validate the

equilibrium void distribution model used in CTF by benchmarking it against the void distribution measurements published by R. W. Sterner and R. T. Lahey, Jr in the NUREG-CR-3373 report "Air/Water Subchannel Measurements of the Equilibrium Quality and Mass Flux Distribution in a Rod Bundle" [1]. The purpose of this validation is to assess the applicability and accuracy of the existing void drift model within CTF. Adding these test cases to CTF's validation suite is important for the purpose of quantifying CTF's effectiveness at modeling the void drift phenomenon.

CTF is a thermal-hydraulic (T/H) simulation sub-channel code designed for light water reactor (LWR) vessel analysis, which uses a two-fluid, three-field (liquid film, liquid drops, and vapor) modeling approach [2]. CTF is based on the COBRA-TF (Coolant-Boiling in Rod Arrays - Two Fluids) code and is being jointly maintained and developed by The Pennsylvania State University Reactor Dynamics and Fuel Management Research Group (RDFMG) and Oak Ridge National Laboratory for use in the Consortium for Advanced Simulation of Light Water Reactors (CASL) [3].

The lateral void drift phenomenon acts to drive vapor to the subchannels with larger flow area. Within CTF, a simple model proposed by Levy and Lahey is implemented with the basic assumption that the fully-developed void fraction distribution is proportional to the fully-developed equilibrium mass velocity distribution. This assumption is indicative of the observation that higher void fractions are found in channels with higher mass velocity [4].

2. EXPERIMENT DESCRIPTION

The experiment being modeling in this simulation was performed as described in Reference 1, and the purpose of this discussion is to outline the bases for the decisions made in the modeling process. The intended purpose of this experiment was to investigate the fully developed two-phase flow distribution in a 2x2 rod array test section. The test facility included a 36 inch long unheated 2x2 rod bundle with an air-water mixture as the working fluid. With a bundle hydraulic diameter of 0.914 inches, a length-to-diameter factor of 39 was calculated, leading to an expected fully-developed flow condition at the bundle outlet. Four 0.055 inch thick 314 stainless steel tubes with 1.0 inch outer diameter were used to simulate the fuel rods. The wall thickness ensured a vibration-free environment during the experiment, and a lower tie plate provided support for the rods. No spacer grids were used in this experiment. In order to realistically simulate boiling, two different techniques were used to distribute the air into the bundle inlet, a sinter sections technique and a mixing tee technique.

Uncertainties within this experiment were measured with the theory of propagation of errors, which is based on the assumption of independent errors. The three independent variables in the error analysis were the subchannel liquid flow rate (Q_{li}), air flow rate (Q_{gi}), and inlet pressure (P_{in}). Uncertainty intervals for each of these three variables were evaluated and used to derive the void fraction error interval, which was calculated for each data point using Equation 1. The coefficients found in this equation were derived from the expressions used for the measured values (i.e., the total mass flux for a given subchannel is an analytical function of liquid volumetric flow rate, air volumetric flow rate, inlet pressure, and flow area). Using this expression, the errors in the subchannel void fractions were found to be no greater than ±6.0% void (not relative), which are represented by the dotted lines found in Figures 5, 6, 7, and 8.

$$\Delta\alpha_i = \pm \frac{\left[2.1X10^{-6}Q_{gi}^2+\left(1.16X10^{-4}Q_{li}+0.075A_i\right)^2\right]^{\frac{1}{2}}}{\left\{0.343Q_{gi}+0.046Q_{li}+29.02A_i\right\}^2} \quad (1)$$

The sinter section technique involved feeding the air at the upper tie plate, which was located at the bundle outlet, through the interior of the rods to sinter sections at the base of each rod. Each rod had its

own separately controlled sinter section so that any number of the four rods could be supplied with air to simulate boiling. The cross sectional schematic of the sinter section can be found in Figure 1.

The mixing tee technique involved soldering thin slabs of sintered metal over cutouts in the water supply line for the test section. An air annulus was constructed to surround the porous section of the pipe, which allowed the air to be bubbled into the mainline. The result was again a two-phase flow mixture at the test section inlet. The cross sectional schematic of the mixing tee setup can be found in Figure 2.

In order to measure the void in each subchannel at the bundle outlet, one of each type of subchannel (corner, side, and center) were physically separated by means of 0.020 inch thick splitters located two inches from the test section outlet. These isolated subchannels were then simultaneously isokinetically sampled to determine the subchannel flow qualities according to Equation 2, where G_g and G_l refer to the water and air mass fluxes, respectively.

$$\langle \vec{x} \rangle = \frac{G_g}{G_l + G_g} \tag{2}$$

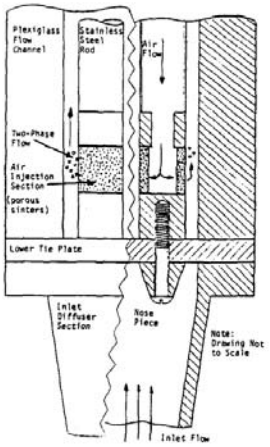

Figure 1. Lower Assembly Test Section with Sinter Section Shown [1]

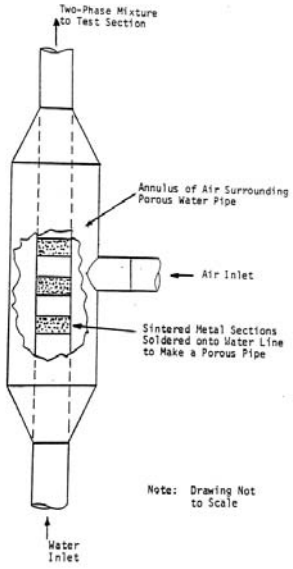

Figure 2. Air/Water Mixing Tee [1]

The subchannel void fraction and quality are related by the Zuber-Findlay equation as found in Equation 3, where $\boldsymbol{\rho_g}$ and $\boldsymbol{\rho_l}$, G, $\langle \boldsymbol{x} \rangle$, $\boldsymbol{V_{gj}}$, and $\boldsymbol{C_0}$ refer to the air and water densities, mass flux, quality, drift velocity, and void concentration parameter, respectively. The void concentration factor depends on the velocity and flow-pattern profiles.

$$\langle \boldsymbol{\alpha} \rangle = \frac{\langle x \rangle}{\left\{ C_0 \left[\langle x \rangle + \frac{\rho_g}{\rho_l} (1 - \langle x \rangle) \right] + \frac{\rho_g V_{gj}}{G} \right\}} \tag{3}$$

The to-scale cross-sectional drawing of the test bundle can be found in Figure 3. The dimensions of this test section are twice that of a typical square pitched BWR fuel rod bundle in order to partially accommodate for the large bubble sizes present with the low pressure air-water experiment. The geometric dimensions used for each subchannel in the experiment and CTF simulations are found in Table I. The different flow area values for these three subchannel types suggest that a below average void fraction would be measured in the corner and an above average void fraction would be measured in the center in the presence of a void drift mechanism. Subchannels 1, 2, and 3 were chosen to be isokinetically sampled to obtain void distribution data for the corner, side, and center subchannel types, respectively.

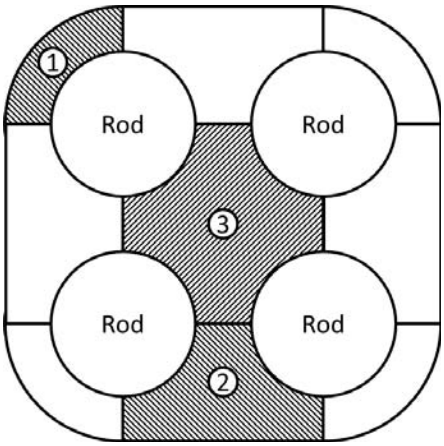

Figure 3. Experimental Cross-Sectional View [1]

Table I. Subchannel Flow Dimensions

Type	Flow Area (in^2)	Hydraulic Diameter (in)
Corner	2.08	1.59
Side	4.68	2.50
Center	7.13	3.57
Total	34.14	2.32

The two-phase void distribution runs from the experiment, Cases 3 through 14, were chosen as the basis for validation in CTF. The operating conditions for these experiments can be found in Table II, which include the water mass flux (G), bundle averaged void fraction $\langle \bar{\alpha} \rangle$, and inlet pressure (P_{in}). The fluid for

all of the experiments was at ambient temperature. Besides the aforementioned four rod experiments, there were also a set of single phase experiments and two-phase single rod experiments described in the report. The single phase experiments were not modeled in CTF since void drift data could not be obtained for this validation. The two-phase single rod experiments were conducted to observe the void drift phenomenon while only using the sinter section of one rod. These experimental runs were not modeled in CTF. The experimental results for these runs can be found in Table III. The corner subchannel void fraction is below the bundle average while the side subchannel void fraction is near bundle average and the center subchannel void is above bundle average, which is expected in the presence of a lateral void drift mechanism.

Table II. Experimental Operating Conditions [1]

Case	$GX10^{-6}\left[\frac{lbm}{ft^2\ hr}\right]$	$<\bar{\alpha}>$ [%]	$P_{in}\ [psig]$	Mixing Technique
3	0.333	20.4	6.0	Mixing Tee
4	0.333	32.8	6.5	
5	0.333	46.1	8.0	
6	0.666	23.6	15.5	
7	0.666	37.5	19.0	
8	0.666	52.7	26.0	
9	0.333	20.4	6.0	4 Sinter Sections
10	0.333	32.8	6.3	
11	0.333	46.1	8.0	
12	0.666	23.6	15.5	
13	0.666	37.5	19.0	
14	0.666	52.7	29.5	

Table III. Experimental Results with Each Mixing Technique [1]

Case	Bundle Averaged Void (%)	Corner Void (%)	Side Void (%)	Center Void (%)	Mixing Technique
3	20.4	14.13	20.94	30.96	Mixing Tee
4	32.8	25.04	32.40	37.23	
5	46.1	37.10	45.88	52.25	
6	23.6	19.56	24.02	26.53	
7	37.5	30.40	36.50	46.67	
8	52.7	42.65	53.66	60.09	
9	20.4	16.02	20.88	29.15	4 Sinter Sections
10	32.8	22.70	32.80	38.88	
11	46.1	36.50	46.07	51.96	
12	23.6	15.34	23.75	29.48	
13	37.5	27.70	35.87	48.85	
14	52.7	39.24	53.19	62.76	

3. CTF SIMULATION CONDITIONS

The experimental test section was modeled in CTF for six different test runs. The number scheme for this geometry can be found in Figure 4. The geometry was then axially discretized into 30 nodes. Since CTF does not directly solve the noncondensable gas equations, the air in the air-water experiments was instead modeled as water vapor. The CTF inlet enthalpy of the two-phase mixture was set to the saturated conditions necessary to achieve the experimental bundle averaged void fraction at the outlet of the experiment while operating at 100 bars. The CTF pressure was changed to 100 bars since convergence issues were present due to the low experimental pressures and high bundle void content. Future work concerning this validation will include either working towards simulations using near-experimental pressures and/or improving on CTF's handling of noncondensable gases. Additionally, it is anticipated that using vapor in place of air in the CTF model will lead to increased uncertainty in the predicted void distributions due to differences in fluid properties and interfacial forces.

Each of these test runs were compared to both the mixing tee and sinter section experiments (i.e., CTF Run 1 is compared to experimental Runs 3 and 9). The void drift option in CTF was then turned off and the simulations were rerun. These runs were also compared to the experimental runs to isolate the effect of the void drift option. Due to the symmetry of the experimental geometry, it was assumed that the corner void measurements (subchannels 1, 3, 7, and 9) were equivalent as well as the side void measurements (subchannels 2, 4, 6, and 8).

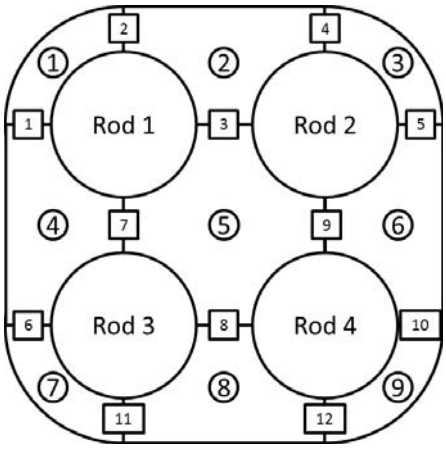

Figure 4. CTF Numbering Scheme

4. RESULTS

The CTF results can be found in Table V. The comparisons between the void drift enabled data and the experimental results can be found in Figures 5 and 6, while the comparisons between the void drift disabled data and the experimental results can be found in Figures 7 and 8. The CTF simulations with void drift enabled appear to agree noticeably better with the experimental results than do the CTF results with void drift disabled. For both sets of comparisons, CTF consistently overpredicts the corner subchannel void and underpredicts the center subchannel void, which reduces the spread of the void distribution, but the expected void drift trend is still visible.

For this comparison, the relative root mean square error (rRMS) is calculated for both the mixing tee and sinter section comparisons using Equation 4. The average rRMS is then calculated for both mixing techniques and compared. Additionally, the average absolute error as calculated in Equation 5 is calculated for each subchannel type for the two mixing techniques. These two error evaluations are

performed for the CTF results with the void drift option enabled and disabled. The summarized results can be found in Table IV.

$$rRMS = \sqrt{\frac{4\left(\frac{\alpha_{CTF}-\alpha_{EXP}}{\alpha_{EXP}}\right)^2_{corner} + 4\left(\frac{\alpha_{CTF}-\alpha_{EXP}}{\alpha_{EXP}}\right)^2_{side} + \left(\frac{\alpha_{CTF}-\alpha_{EXP}}{\alpha_{EXP}}\right)^2_{center}}{9}} \quad (4)$$

$$\overline{\epsilon_{abs}} = \sum_{i=1}^{n} \frac{(\alpha_{CTF}-\alpha_{EXP})_i}{n} \quad (5)$$

From the error summary, it is clear that having the void drift option enabled caused significantly less error than when it is disabled. As for the mixing technique, both methods had similar errors, but the mixing tee technique was consistently more accurate than the sinter sections technique. When taking into account the average absolute errors, the same trend as with rRMS is present, where an enabled void drift option with mixing tee is the most accurate case. In each category, the void fraction in the corner subchannel was overpredicted, and the void fraction in the center subchannel was underpredicted. Additionally, the side subchannel consistently had the least error.

When taking into account the experimental error interval, the average absolute error values for when void drift is enabled are well below the ±6% threshold. Conversely, the absolute error values for when void drift is disabled are above the experimental error interval mark for both the corner and center subchannels. However, the side subchannel in this case has very little error, which can be attributed to the side subchannel void fraction being near the bundle average value for both the experimental and CTF results.

Table IV. Error Summary

Void Drift Option	Mixing Technique	rRMS	Average Absolute Error (%)		
			Corner	Side	Center
Enabled	Mixing Tee	0.1369	5.4167	0.5167	4.6617
	Sinter Sections	0.1687	6.3333	0.4533	5.4333
Disabled	Mixing Tee	0.2185	8.0533	0.6333	6.5383
	Sinter Sections	0.2804	9.9500	0.7033	7.7633

As previously mentioned, the CTF input was rerun with the void drift option disabled in order to isolate the effects of CTF's void drift option. As seen in Table V, there is no consistent trend with these results as was found when the void drift was enabled. The void fraction in each subchannel type does not deviate much from the bundle average value as it did with the void drift option enabled. There was a noticeable increase in error with the cases run without the void drift model compared to the cases with the void drift model.

Table V. CTF Results

Case	Void Drift Option Enabled			Void Drift Option Disabled			Mixing Technique
	Corner Void (%)	Side Void (%)	Center Void (%)	Corner Void (%)	Side Void (%)	Center Void (%)	
3	18.50	20.60	22.10	21.90	20.40	19.60	Mixing Tee
4	21.80	32.80	39.10	34.90	32.30	31.90	
5	28.70	45.80	54.80	47.00	45.30	46.60	
6	22.40	23.70	24.90	24.30	23.40	23.80	
7	34.10	37.60	40.70	37.20	37.30	38.70	
8	48.50	52.70	56.30	51.90	52.50	53.90	
9	18.50	20.60	22.10	21.90	20.40	19.60	4 Sinter Sections
10	21.80	32.80	39.10	34.90	32.30	31.90	
11	28.70	45.80	54.80	47.00	45.30	46.60	
12	22.40	23.70	24.90	24.30	23.40	23.80	
13	34.10	37.60	40.70	37.20	37.30	38.70	
14	48.50	52.70	56.30	51.90	52.50	53.90	

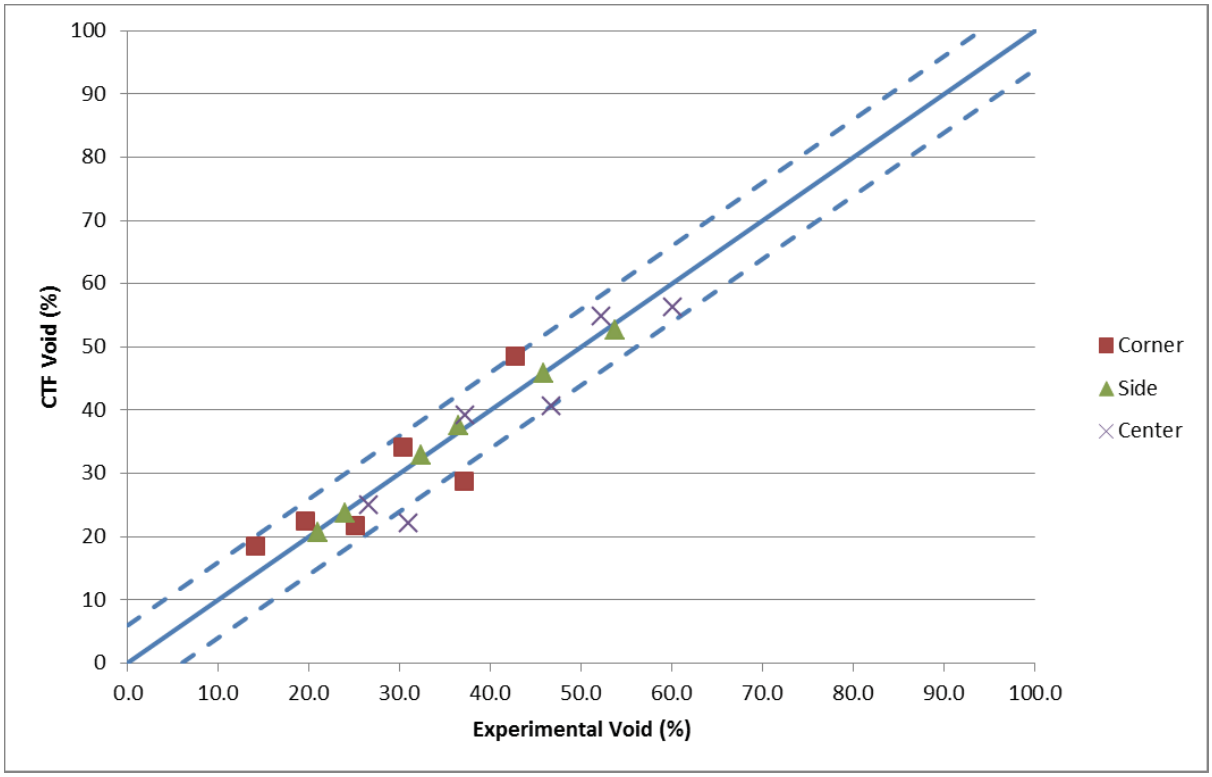

Figure 5: CTF-Experiment Agreement (Mixing Tee) with Void Drift Enabled

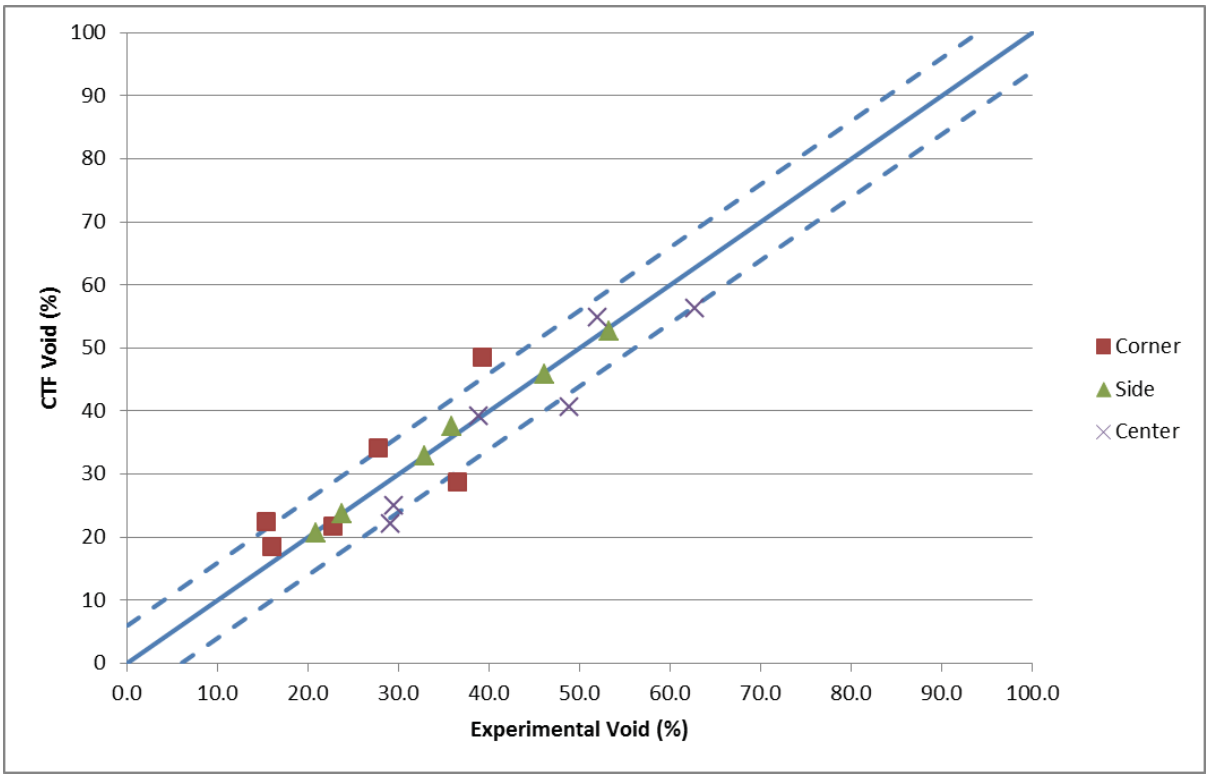

Figure 6: CTF-Experiment Agreement (Sinter Sections) with Void Drift Enabled

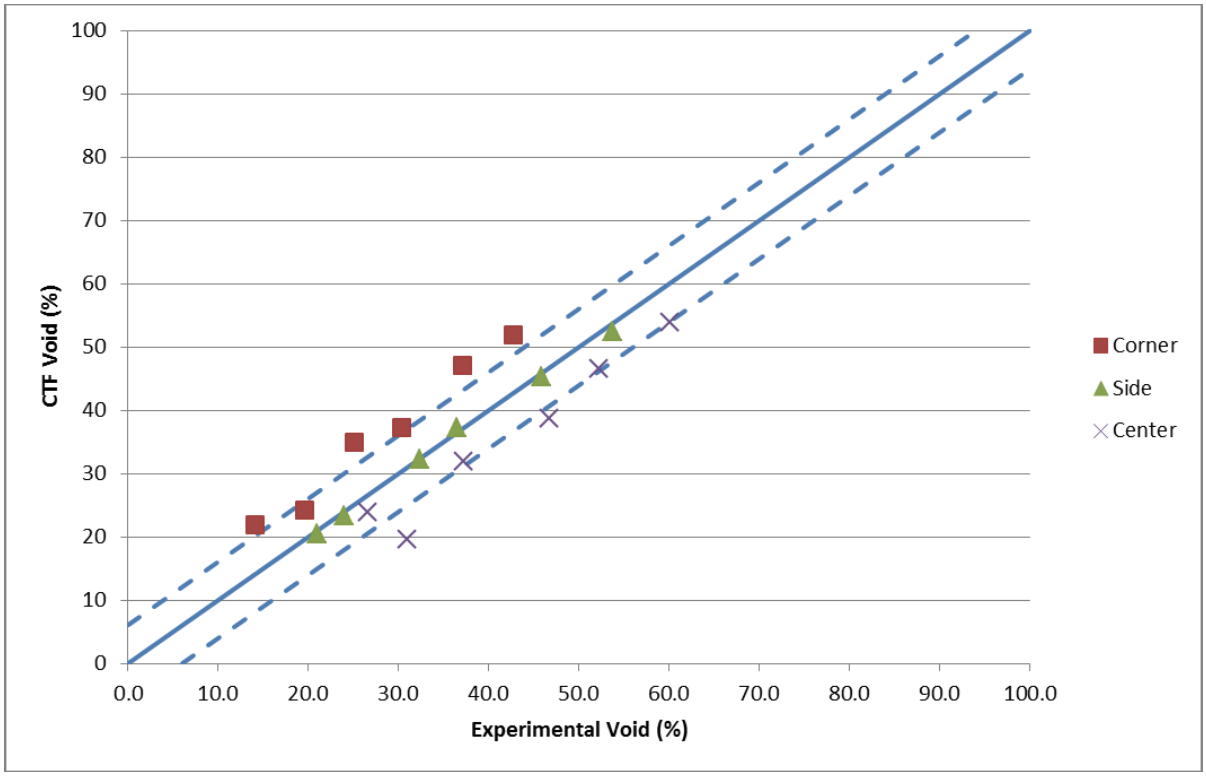

Figure 7: CTF-Experiment Agreement (Mixing Tee) with Void Drift Disabled

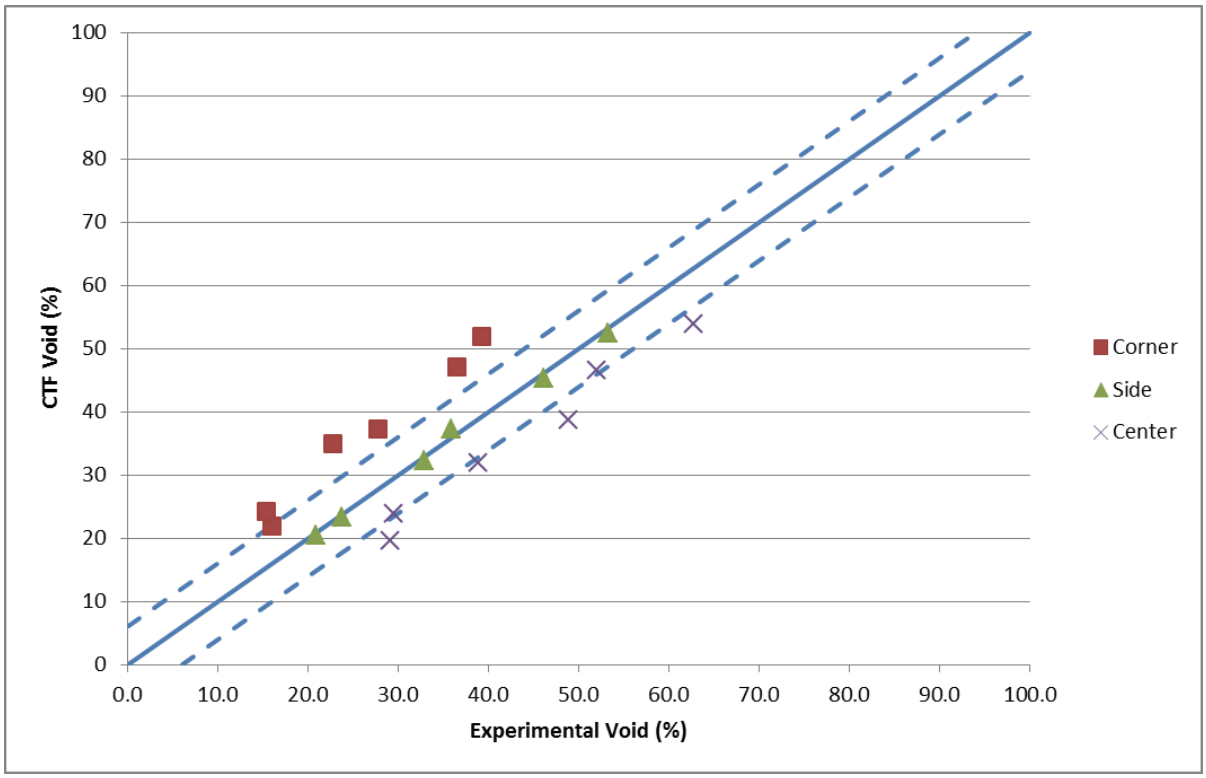

Figure 8: CTF-Experiment Agreement (Sinter Sections) with Void Drift Disabled

In order to further verify that the desired trend is captured in CTF's void drift option, the subchannel void fractions for when the void drift option is enabled and disabled are plotted against the bundle average void fraction in Figures 9 and 10, respectively. When the void drift option is enabled, it is clear that the center subchannel always has the highest void while the corner subchannel always has the lowest. It is also worth noting that the spread of the void data tends to be much larger for the experimental runs with the lower mass flux. Therefore, the expected void drift trend is present. When the option is disabled, however, the corner, side, and center subchannel void fraction are all very close to the bundle average with no clear trend. For this case, there is no lateral void drift, and the subchannel void remains mostly unchanged axially and laterally. The reason for the void distribution not being exactly uniform in this case is likely due to the convergence criteria used for this validation study.

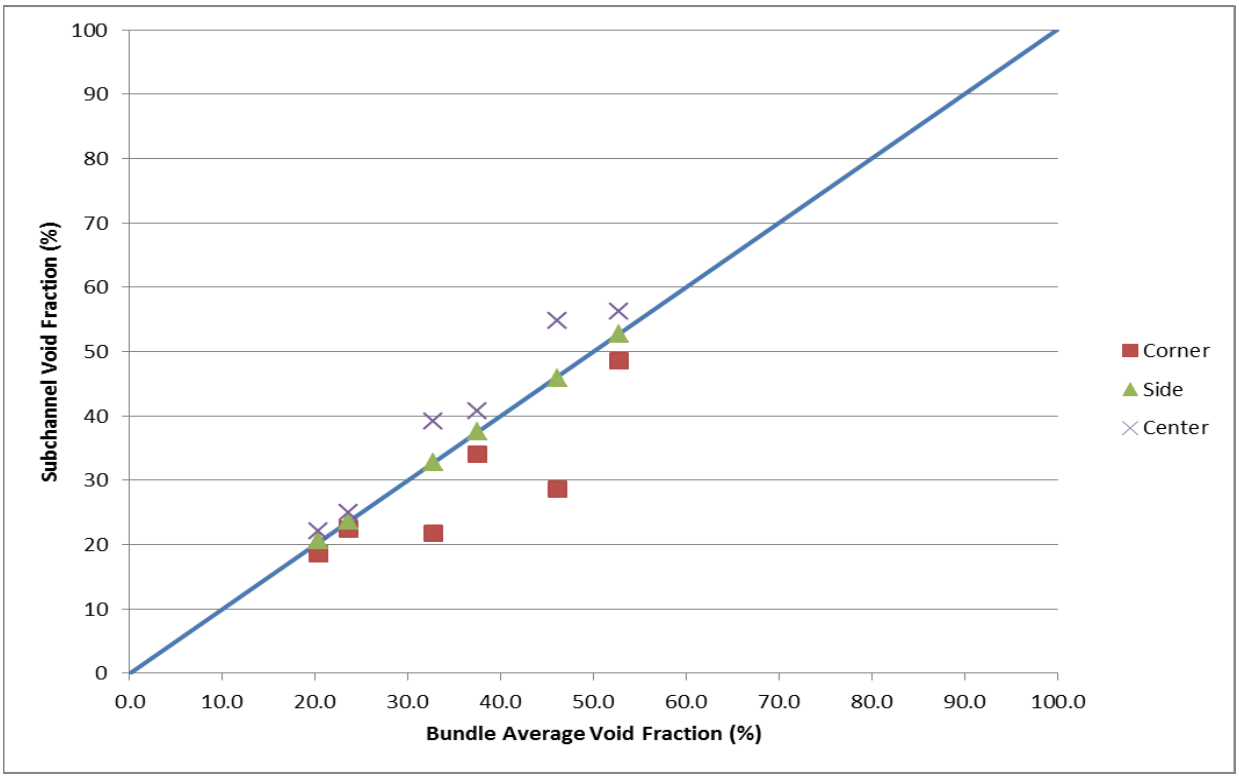

Figure 9: Void Distribution with Void Drift Option Enabled

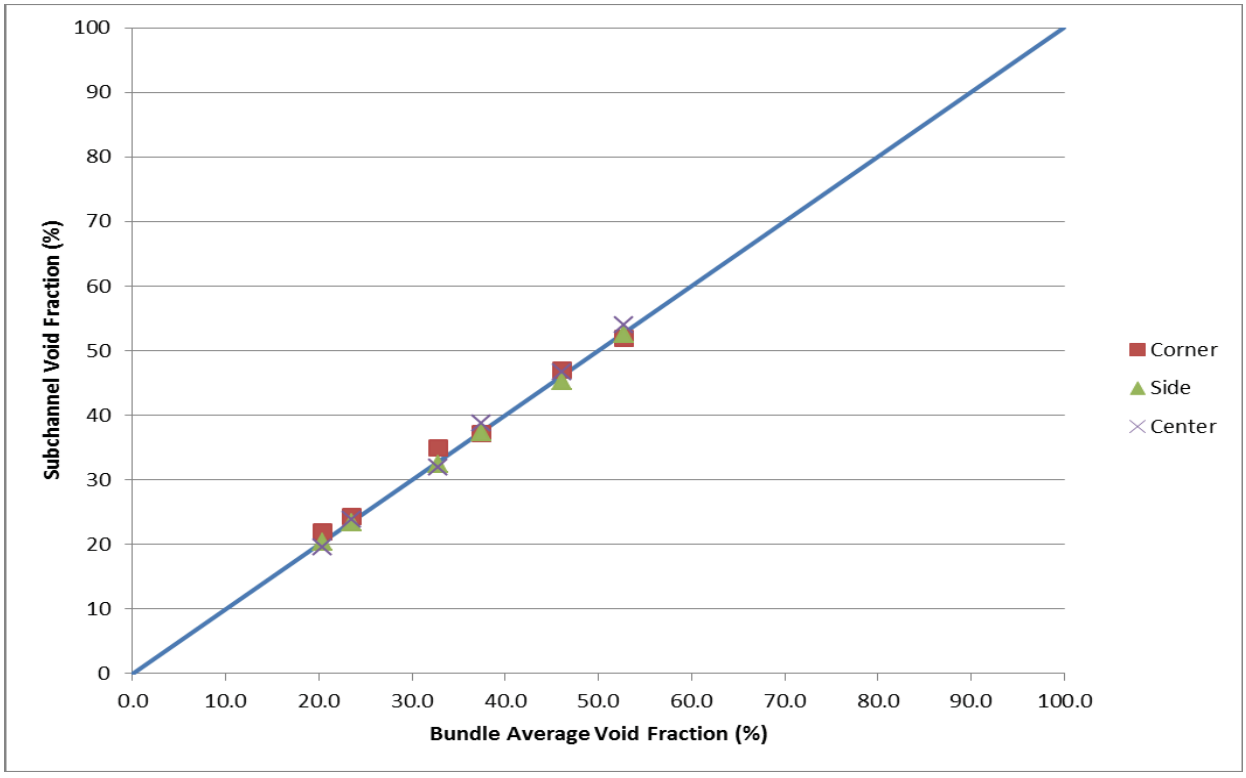

Figure 10: Void Distribution with Void Drift Option Disabled

5. CONCLUSIONS

The CTF results calculated with the void drift option enabled exhibits the same trend as found in the NUREG/CR-3373 report, which experimentally demonstrates the presence of a lateral void drift mechanism. The corner subchannel void is consistently overpredicted while the center void is consistently underpredicted, however, as summarized in Table IV, the CTF-experiment error is consistently within the ±6% error interval when the void drift option is enabled. Conversely, the error is outside of this experimental uncertainty when the void drift modeling option is disabled. The rRMS values with the void drift option enabled were significantly less than those with the void drift disabled with the void drift enabled mixing tee and sinter section rRMS being 0.1369 and 0.1687, respectively, and the void drift disabled mixing tee and sinter section rRMS being 0.2185 and 0.2804, respectively.

From these results, it can be concluded that CTF's void drift model as adapted from Lahey and Levy's simple model simulates a lateral void drift phenomenon similar to the distributions described in the NUREG/CR-3373 report. Further work for this validation includes simulating additional void drift experiments in order to validate CTF's ability to simulate void drift. Considering the necessity of using saturated steam in these simulations as opposed to the air used in the experiments, any additional validation work with CTF's void drift model would likely involve experiments using steam as opposed to air or the further development of CTF's applicability with air as a working fluid

ACKNOWLEDGMENTS

This template was adapted from the template for M&C + SNA 2007 posted on the Internet. This material is based upon work supported by The Consortium for Advanced Simulation of Light Water Reactors (CASL).

REFERENCES

1. Sterner, R. W., & Lahey, Jr., R. T. (1983). Air/Water Subchannel Measurements of the Equilibrium Quality and Mass Flux Distribution in a Rod Bundle (NUREG/CR-3373). Rensselaer Polytechnic Institute.
2. Salko, R. K., & Avramova, M. N. (2014). *CTF Theory Manual.*
3. Paik, C. Y., Hochreiter, L. E., Kelly, J. M., Kohrt, R. J., Westinghouse Electric Corp., & Battelle Northwest Laboratory. (1985). *Analysis of FLECHT-SEASET 163-Rod Blocked Bundle Data using COBRA-TF (NUREG/CR-4166).*
4. Lahey, Jr., R. T., & Moody, F. J. (1993). *The Thermal-Hydraulics of a Boiling Water Nuclear Reactor.* American Nuclear Society.